

Spectroscopic techniques for corrosion detection using drones

Technology review as part of work within the performance contract “Dronemetrologi”



Hugo Kerdoncuff, Wan-Ing Lin, Lars Johann Wacker

Spectroscopic techniques for corrosion detection using drone
Technology review as part of work within the performance contract "Dronemetrologi

Report DFM-2017-R005, Ver. 1.01
2017

By
Hugo Kerdoncuff, Wan-Ing Lin, Lars Johann Wacker

Copyright: Reproduction of this publication in whole or in part must include the customary
bibliographic citation, including author attribution, report title, etc.

Published by: DFM A/S, Kogle Allé 5, 2970 Hørsholm
Denmark

Request report
from: www.dfm.dk

Content

1.	Introduction.....	5
1.1	Legal and technological framework.....	5
1.2	Sensor requirements for drone deployment.....	6
1.3	Requirements for efficient corrosion detection.....	7
1.4	Requirements for detection accuracy.....	7
2.	Spectroscopic methods for corrosion detection.....	8
2.1	Microwave and millimetre-wave imaging.....	8
2.2	Terahertz spectroscopy.....	10
2.3	Infrared thermography.....	12
2.4	Fourier-transform infrared spectroscopy (FTIR) / Mid-Infrared spectroscopy (MIR).....	13
2.5	Colour, multispectral, and hyperspectral imaging and VIS-NIR spectroscopy.....	15
2.6	Raman spectroscopy.....	18
2.7	Laser-induced breakdown spectroscopy (LIBS).....	18
2.8	X-ray spectroscopy.....	20
3.	Evaluation and conclusion.....	21
4.	Bibliography.....	25
5.	Acknowledgements.....	29

Summary

Corrosion is one of the major cost factors in the inspection and maintenance of offshore structures and in particular for wind turbines. Inspections require rope access teams, which is time consuming, costly and imposes safety issues. Replacing these inspections by drone-based operations will thus be beneficial on many levels.

Current state-of-the-art inspections using drones rely on footage from colour cameras. This method requires the subsequent rating of the images by specially trained inspectors, which is inherently prone to uncertainty and large variations of the rating due to subjectivity.

This review aims to identify the technical requirements and possibilities for operating a corrosion sensor from a drone platform, which would deliver objective ratings of the state of an asset without the help of a human inspector.

Specifications of current state-of-the-art drone platforms set requirements for the sensor, which corresponds to a maximum weight of 1.5kg, a maximum size of 240 mm x 160 mm x 130 mm, and a maximum average power consumption of 100W. Moreover, the sensor needs to be working in a non-contact, non-destructive way with a detection range of minimum 3 m. Inherent limitations of the drone platforms like mechanical vibrations are only discussed qualitatively. According to current regulations and industry needs, the measurement uncertainty of the corrosion sensor should be no higher than 5%.

This review focusses on spectroscopic solutions, since they demonstrate a high specificity to chemical compounds and elements, which is necessary for detecting corrosion products. Different options are discussed in terms of sensing capabilities, and operational and technical requirements for implementation on a drone. These methods include microwave spectroscopy, terahertz spectroscopy, infrared thermography, Fourier-transform infrared spectroscopy, infrared spectroscopy, visible to near-infrared spectroscopy, colour imaging, multi- and hyperspectral imaging, Raman spectroscopy, laser-induced breakdown spectroscopy and X-ray spectroscopy.

In conclusion, we find a poor technological fitness for this application for microwave-, terahertz, Fourier-transform, Raman and X-ray spectroscopy. Infrared, visible to near-infrared spectroscopy, colour imaging, hyperspectral imaging and laser-induced breakdown spectroscopy are identified to have fair technological suitability. Infrared thermography and multispectral imaging are found to be the most feasible technologies considered in this review.

Review of spectroscopic methods for the detection of corrosion using drones

1. Introduction

Corrosion represents a major cost factor for modern societies. Estimates attribute about 3.4 % of the world wide gross domestic product to costs related to corrosion¹. The degradation of steel structures has multiple effects ranging from a purely cosmetic issue of red rust stains on painted surfaces to severe structural collapses. A constant monitoring of critical structures such as buildings, bridges and towers is thus of outmost importance for the safety of the structures.

However, many of these structures are found in remote locations, like offshore wind turbines and oil and gas drilling platforms, or raise safety issues in case of inspection, e.g. due to their heights. Other issues include necessary transportation pathway closedown in case of inspection of public transport infrastructures such as bridges, which leads to high associated cost and inconvenience for the public. The use of drones is an efficient way to inspect hardly accessible structures. It provides both increased safety during operation and inspection, and reduced associated maintenance costs. Currently, the use of drones for maintenance inspection is limited to the acquisition of camera footage, which is subsequently rated by specialists. This evaluation method is cost intensive and depends highly on the experience and subjectivity of the inspector.

This report will focus on corrosion detection and evaluation beyond the state-of-the-art and tries to identify corrosion detection methods that could be deployed on a drone. Ideally, the identified method shall be able to quantify the amount of corrosion without the external help of a human inspector, or at least guide the inspector with suggestions for a more efficient and objective inspection. Due to the airborne nature of the drone platform, the review will focus on non-destructive, non-contact and remote methods. Most spectroscopic methods answer these criteria and can furthermore provide chemically specific information, which makes them good candidates for corrosion detection and evaluation. Since monitoring corrosion is essentially an industrial need, the use of professional drones with their associated higher load capabilities will be assumed in this report.

The report is structured as followed. First a technological review of payload mass, dimension and other restrictions is given. In the second part, the requirements for a corrosion sensor are laid out in terms of current norms. The following part describes the different spectroscopic solutions available and evaluates them in terms of their applicability for drone-based corrosion detection. The last part compares the different methods and rates their feasibility.

1.1 Legal and technological framework

Danish legislation defines five categories for unmanned aerial vehicles (UAV). These categories are differentiated by weight as shown in Table 1. Drones of category 3 are not exempted from some of the regulations for manned aircraft as drones of the other four categories are. This makes operation in general more difficult and less attractive for inspection enterprises. For professional use, only drones of category 1B, 2 and 3 are of importance. UAVs with a maximum take-off weight (MTOW) lower than 1.5 kg only allow for very small payloads and will thus not be considered within this framework. Therefore only drones of category 1B and 2 are reasonable choices for professional corrosion inspection applications with associated payloads ranging from 1.5 kg to 10 kg. Further legal constraints like minimum distances to built-up areas are not considered here due to the technical nature of this review.

Category	Typical usage	MTOW	Typical payload	Comments
Microdrone	Recreational use	250 g	NA	Not considered in this review because of limited payload
1A	Recreational use, aerial photography	1.5 kg	Normally only RGB camera	Not considered in this review because of limited payload
1B	Simple commercial use, aerial photography	1.5 to 7 kg	1.5 kg	Typical drone for professional use
2	Advanced commercial use	7 to 25 kg	Typical 5.5 to 10 kg	Large professional drone
3	Commercial use	> 25 kg	Above 10 kg	Not considered in this review because of regulatory constraints

Table 1 Drone categories within Danish aviation law²⁻⁴.

1.2 Sensor requirements for drone deployment

On a global scale, the Chinese company DJI represents the company with the largest market share⁵. Their largest multipurpose drone with gimbal mount is the Matrice 600 Pro, which can carry up to 6 kg of payload⁴. Stabilization mounts like gimbals reduce the allowed payload weight and dimensions to about 1.5 kg and 240 mm x 160 mm x 130 mm. Within this report, these specifications are considered as representative for most drones.

Due to expected miniaturization at a later stage of technological development, the requirements for the payload dimensions and weight are relaxed to a footprint of 25cm x 25 cm with a mass of about 1.5 kg in accordance with the requirements laid out in the underlying result contract of this report⁶.

The airborne nature of the sensor imposes additional constraints related to positioning and pointing stability, vibrations, distance to the target area and available time for a measurement. Current state-of-the-art flight control systems⁷ specify a hovering performance of 0.02 m vertically and 0.01 m horizontally when using the Global Navigation Satellite System (GNSS). With the Global Positioning System (GPS) for navigation alone the accuracy reduces to about 0.5 m vertically and 1.5 m horizontally. For safe operation in case of navigation system failure the drone should hold a minimum horizontal distance of 3 m, which sets a lower limit to the measurement distance. Data on vibrations from the drone relevant for the measurement is not available. Subsequently the issue is considered only relevant for high precision and high-resolution measurements. By employing market available gimbal mounts⁸ to reduce vibrations and pointing variations, the pointing instability can be reduced to $\pm 0.02^\circ$. Combining the pointing and positioning stability results in an uncertainty of the measurement position on the object of about 9 cm.

Typical multirotor drones carry batteries with a capacity of about 100 Wh for flight times of about 16 minutes⁴. Assuming an acceptable reduction of the flight time by 25%, the average power consumption of the sensor should not exceed about 100 W when using the on-board battery.

1.3 Requirements for efficient corrosion detection

Corrosion is defined as a process of changing the properties of a building material from its design specifications. While corrosion is mostly considered as the loss of bearing material caused by oxidation, this review will also consider the detection of the corrosion products. In terms of structural construction, the most prominent products are metal oxides originating from steel or aluminium. Since corrosion in aluminium is normally prohibited by a protective aluminium oxide layer, which forms naturally at the surface, we will rather focus on steel corrosion products and their detection, if not stated otherwise.

Different corrosion detection and quantification methods are currently used. Most steel surfaces are covered with protective coatings and paints, which prevent corrosion, but tend to mask the apparition and spreading of corrosion in case the protective layers are breached. Most non-destructive evaluation methods focus on measuring the loss of material. However, the detection of a breakdown or end-of-life of the protective coating, or the detection of corrosion products are already good indicators for maintenance decisions.

The identification of oxidation products is often complicated as the earliest corrosion products are usually not in their most stable state and may undergo conversion. Detectable products include, amongst others, $\text{Fe}(\text{OH})_x$, FeOOH , $\gamma\text{-FeOOH}$, $\alpha\text{-FeOOH}$ and Fe_3O_4 ⁹.

The most common methods for the detection and evaluation of corrosion are manual inspection and manual rating of images of the sample by a specialist. Most standards require comparing the state of the asset with reference images and rating the surface condition in respect to parameters such as blistering and amount of rust. This procedure is prone to a high variability in the ratings due to the subjectivity of the specialists. Different approaches have aimed at removing subjectivity by using computer algorithms and are discussed in the section on colour imaging methods.

1.4 Requirements for detection accuracy

The main standards for the assessment of degradation of coatings and corrosion on surfaces are ISO-4682¹⁰, ASTM D610¹¹ and the "European scale of degree of rusting for anticorrosive paints"¹². These standards list surface conditions into six to eleven categories. For example, ISO-4682 ranks surface conditions into six categories from 0 to 5, with a rating of 0 corresponding to an undamaged sample and a rating of 5 to a severely corroded sample. While the nomenclature of the categories might be different between standards, the due time for maintenance is usually considered at around 1% surface deterioration, and the maximum amount of surface deterioration for a localized repair is about 3 to 5%¹³. Considering the higher costs of non-localized repairs, a valuable corrosion sensor should be able to measure surface deterioration below 5%. Additionally, the standards not only take into account the total corroded area (ISO 4628-3) but also the size of the single defects (ISO 4628-2). The end-of-life of protective coatings is attributed to category 2 to 3, while localized repairs are possible up to category 4. Damages corresponding to category 3 involve a total percentage of rusted area up to 1% and defect sizes of 0.5 to 5 mm. Category 4 allows for maximum 8% of rusted area and defect sizes larger than 5mm, which is considerably easier to detect. In this report, we will assess the corrosion detection and evaluation methods in regards to their ability to detect surface damages of category 3.

2. Spectroscopic methods for corrosion detection

This section describes different spectroscopic methods to detect corrosion or corrosion products. The focus lies mainly on corroded steel, where not mentioned differently. While many common detection methods like ultrasound or eddy current detection have been widely adopted by industry and might be superior by performance compared with the techniques discussed in this review, they disqualify in the context of remote corrosion sensing from a drone, since the probe needs to be in contact with the sample. As such, less obvious choices for inspection are also discussed as they might be able to fill this gap.

Most spectroscopic methods do not require contact with the sample. However, some may have long recording times or need high collection efficiencies, among other drawbacks. These requirements and the efficiency in identifying and quantifying corrosion are discussed in this section together with more basic technical requirements for the use on a drone.

While spectroscopic methods are often associated with the analysis of visible light that has been interacting with a sample, this report considers the definition of spectroscopic methods in a very broad sense. This includes techniques like time-domain spectroscopy or x-ray fluorescence spectroscopy. Most of the techniques are discussed from a measurement point of view. However, in the case of inspections using cameras the analysis with advanced analytical methods is also considered, since the combination would fulfil most requirements stated above.

This section includes reviews on microwave and millimetre-wave imaging, terahertz-spectroscopy, infrared imaging and thermography, Fourier-transform infrared spectroscopy, spectroscopy in the visible region, overlapping with colour as well as multi- and hyperspectral cameras, Raman spectroscopy, laser-induced breakdown spectroscopy and finishes with x-ray spectroscopy techniques. While this section only focusses on the methods on their own, the following section will compare the different methods with each other and conclude the report.

2.1 Microwave and millimetre-wave imaging

Microwave imaging is a non-destructive, non-contact imaging technique, which employs microwave radiations to image inhomogeneities and interfaces in materials. It relies on the changes in diffusion, absorption and reflection of microwave radiations that occur due to variations of electromagnetic properties in materials. Microwaves span frequencies in the 300 MHz to 300 GHz range, which correspond to wavelengths from 1 mm to 1 m. Compared to visible and infrared radiations, microwaves can penetrate deeper in most materials. Therefore microwave imaging has many diverse applications for material characterization, non-destructive testing and evaluation of dielectric and composite structures¹⁴, evaluation of thick coatings¹⁵, civil structure monitoring¹⁶, but also in healthcare and biosensing¹⁷, as well as screening at airport security¹⁸, where millimetre-resolution is sufficient.

In its simplest configuration a microwave imaging system consists of one microwave antenna acting as both emitter and receiver, a signal processing unit controlling the emission and acquisition of the microwave signal (e.g. Network analyser), and an imaging algorithm reconstructing 2D or 3D images of the observed object (e.g. a synthetic-aperture radar algorithm for 3D images)¹⁹. The frequency range in which the antenna can emit and receive microwaves is determined by its design, with the wavelengths of the microwaves in the order of the antenna size. When designing a microwave antenna for a particular application there is often a trade-off between resolution and penetration depth due to many materials having a stronger absorption at

shorter wavelengths. The varying response of materials to different wavelengths also allows spectroscopic measurements to distinguish between materials in a sample. However, the microwave spectrum of a sample is principally affected by the geometric characteristics of the sample (coating thickness, defect dimensions, etc.) and chemometric methods such as PCA (principal component analysis) must be applied in order to recover information about the materials¹⁵.

Microwave imaging relies on the measurement of coherent properties of the reflected microwave radiations such as magnitude, phase, polarization and frequency, at different positions on the sample. Often, coherent properties of the emitted microwaves must be optimized for a particular application. For example the reflection of microwaves from steel rebars is strongest when the polarization of the microwaves is parallel to a rebar¹⁹.

Compared to common testing and evaluation techniques such as visual inspection, ultrasound, eddy current, and shearography, microwave imaging has the combined advantages of remote detection, detection through materials such as paint and cement, and detection in both dielectric and conductive materials. For these reasons microwave imaging has been extensively investigated for the evaluation of corrosion in composite materials¹⁴, civil structures¹⁶, under paints and coatings^{15,20}, etc. Zhang et al. employed a sweep frequency microwave imaging technique for the evaluation of corrosion on steel under a coating²⁰. Steel samples were exposed to atmospheric corrosion from one to ten months and subsequently coated with 150 μm paint. Corroded areas were imaged by raster scanning the microwave antenna (a centimetre-size open-ended rectangular waveguide) over the sample and recording the averaged magnitude and phase of reflected microwave radiations in an 8.5 GHz range (18 - 26.5 GHz). Another study¹⁹ from Kharkovsky et al. describes a three-dimensional microwave imaging technique for the evaluation of corrosion of steel rebars in cement-based structures. The imaging system is similar to the one from Zhang et al., with the addition of a wideband synthetic aperture radar technique to render three-dimensional images. Rebars were imaged at a depth of 25 mm and 50 mm inside mortar with a spatial-resolution of approximately 5 mm when using microwave radiations in the K-band (18 - 27 GHz). The thinning of rebars and the presence of rust could be observed through the mortar.

Although the evaluation of rust and defects under coatings and inside cement-based structures has been demonstrated experimentally it remains challenging to perform in the field. One of the major obstacle is the control of the standoff distance (distance between the probe and the sample, also called lift-off) which is crucial in reaching optimum sensitivity. With a short standoff distance the system operates in the near field region and becomes more sensitive to variations due to irregular surfaces of the sample or movement of the probe, which are often considered as noise. On the other hand, at large distances the penetration depth decreases. Thus an optimum standoff distance must often be determined theoretically and experimentally for a particular application. In most corrosion evaluations using microwave imaging the standoff distance is set within 1 mm to 10 mm and any variation during measurement may affect significantly the result¹⁶. In order to relax the constraint on standoff distance stability, compensation techniques have been developed: by monitoring the standoff distance then correcting the microwave measurement¹⁴ or by employing differential probes to detect material boundaries²¹. Nevertheless, the required stability remains within a few millimetres.

Imaging systems embarked on drones that employ microwave radiations have already been developed for long-range radar imaging of landscapes and buildings with resolutions on the order of metres. Therefore, it is reasonable to consider that the specifications of a microwave imaging system for corrosion evaluation can be fitted to the size, weight and power requirements of a

drone application. However a major limitation to the application of microwave imaging on drones are the constraints on standoff distance and stability since specifications for drone position stability are usually two orders of magnitude higher than the millimetre positioning required for microwave imaging. As a conclusion, although microwave imaging enables evaluation of rust and defects for civil structures, its practical implementation on drones requires major technological improvement to overcome these constraints.

2.2 Terahertz spectroscopy

The International Telecommunication Union defines terahertz radiation (THz) as electromagnetic radiation with a wavelength of about 0.1 mm to 1 mm²². The photon energy is smaller than the ionization energy of most materials and smaller than the bandgap energy of non-metallic materials. Generally, these materials transmit THz waves, while metals reflect them²³. These properties make THz waves an obvious choice for use within non-destructive testing and evaluation.

There are two types of THz non-destructive evaluation and spectroscopy techniques. Frequency-domain spectroscopy measures the response of the sample for different frequencies of the incoming radiation employing a continuous wave source. Time-domain spectroscopy uses short pulses of radiation, recording the time dependent response. While frequency-domain spectroscopy can determine the material composition of the sample, time-domain spectroscopy detects boundaries and interfaces of different materials and is employed to measure the thickness of material layers, such as coatings.

The two main techniques for the generation of coherent THz radiation are frequency multiplication of radio frequency signals using semiconductor diodes (mostly GaAs-Schottky diodes)²⁴ or frequency division by using two lasers (photo mixing)²⁵. Other methods of THz generation include the use of synchrotron radiation²⁶, free electron lasers (FEL)²⁷, gyrotrons²⁸, backward wave oscillators²⁹, varactor rectifiers³⁰, rectifiers using resonant tunnelling diodes³¹, photo-Dember rectifiers³², far-infrared lasers (quantum cascade lasers³³⁻³⁶ or organic gas far-infrared laser³⁷) and optical rectification emitters³⁸.

Photomixing is the most common technique for time-domain spectroscopy. Two lasers are detuned with respect to each other by the required terahertz frequency and overlapped on a non-linear component to generate the radiation. Time-domain spectroscopy requires ultrashort pulses in the picosecond range and generation is achieved by replacing one of the two lasers in the beat frequency generation scheme by an ultrashort pulse laser.

Equipment for the generation of continuous wave THz radiation is generally available in the size and weight range required for drone deployment. Picosecond pulsed laser sources required for time-domain spectroscopy are not available for in field deployment. Their size and weight exceed the load requirements and their delicate design make them prone to failure due to vibrations on a drone platform.

Detection of THz waves depends on the frequency range. Detection strategies range from phase locked detection of reflected or transmitted signals using a biased photodiode and time gating with ultrashort pulses. Fixed wavelength and broadband detector arrays and cameras are available for certain wavelengths. However, high-sensitivity detection systems might require cryogenic cooling making their use on drones virtually not efficient.

THz radiation testing suffers from two major technological drawbacks. First, the spatial resolution is limited to the radiation wavelength, which is on the order of millimetres. This might prevent the detection of small corrosion defects significantly smaller than the detection wavelengths. Second,

THz technology is not available with high power and efficiency for transmitters and receivers, which limits its sensitivity and makes an integration into a noisy drone environment challenging. Moreover, the available equipment is relatively expensive and heavy and for high sensitivity, the detector needs cryogenic cooling.

However, a number of different approaches to use THz radiation for testing purposes have been evaluated in recent years. For example, to surpass the limited spatial resolution of THz radiation imaging, the use of near field imaging has been demonstrated³⁹ though this technique suffers from a reduced distance between the probe and the sample.

In the aftermath of the 2003 accident of the Space shuttle Columbia, the National Aeronautics and Space Administration in the USA started developing “advanced non-destructive evaluation, totally non-contact, non-liquid coupled techniques to access density variations in the thermal protection foam”. Anatas and Madaras have studied the possibility to detect corrosion with THz radiation on this background and have shown that it is possible to detect corrosion under paint when the paint starts swelling and blistering⁴⁰ and under the isolation tiles of the space shuttle⁴¹. Building on their work Kurabayashi et al.⁴² investigated possible imaging through multi-layered paint using different THz frequencies. They found, that the absorption is highly dependent on the type of paint used and thus different frequencies have to be used for different types of coating. Moreover, the technique might not be applicable when the absorption of the applied coating is too high. Another approach by Anatas and Madaras addresses the problem by measuring the surface roughness under layers of paint⁴³. Their results show potential, but require recording a signal from different angles, making a measurement from a drone too time-consuming.

Another approach is the use of THz spectroscopy to directly detect and determine corrosion products. A proposal for the detection of rust under concrete from the National Institute of Standards and Technology (NIST) suggests detection of an antiferromagnetic resonance in the iron oxides. Studies on rusted steel plates showed great promise⁴⁴. Two recent publications show the identification of goethite via a one and two magnon resonance at about 0.5 and 0.9 THz, respectively⁴⁵ and hematite at low temperatures⁴⁶. Unfortunately, the resonance in hematite is not present at room temperature, since the Morin temperature is about 260 K, making its application in the field impossible.

THz technology has a high potential for corrosion detection. However many issues remain that have prevented the wide spread use for ground inspections making a drone deployment even less likely. Current equipment is costly and heavy. Taking full spectra is slow and thus not feasible for drone integration. The use of coherent THz radiation allows the suppression of the influence from non-coherent radiation like thermal sources. However, the coherence of the radiation can give rise to interference and will require phase control of the source and detector to suppress the detection of interference fringes. The influence of vibrations caused by the nature of the drone platform on the generation and detection would require more elaborate testing and precautions. However, deployment of a simple THz system on a drone has been demonstrated for transmission measurements⁴⁷. Proposed procedures for resonance detection would rely on a system employing the detected resonances by the team at NIST between 0.5 and 1 THz. However, data on detection distances and sensitivities for a drone based THz system are not published and reflection measurements have not been demonstrated to date. Looking at other similar systems on the market, this approach is considered not feasible. Time-domain spectroscopy has been proven to be useful for the determination of coating thickness, which can be a first sign of the protection break down making it a good choice for maintenance inspection. However, current time-domain systems do not comply with the size and weight restrictions inflicted by the drone platform.

2.3 Infrared thermography

Infrared thermography images the temperature of objects via detection of their infrared “blackbody” radiation⁴⁸. All objects emit radiation according to the blackbody radiation law and, at temperatures in the range of -270 °C to 3590 °C, the emission spectrum peaks in the infrared region (0.75 μm - 1000 μm). Near ambient temperatures, a narrower range of detection between 7 μm to 14 μm, referred to as long-wave infrared (LWIR) band, is usually used. In addition to covering the emission peaks of bodies near ambient temperatures (-66 °C to 141 °C), the LWIR band has the advantage of being separated from the main emission band of the sun, which is highly relevant for outdoor measurements. Infrared detectors have seen major improvements in the past two decades⁴⁹ with the development of uncooled micro-bolometers and focal plane arrays (FPA) which enable megapixel two-dimensional infrared imaging. The typical parameters to consider when selecting a thermography system for a particular application are spectral range, temperature range, spatial resolution, temperature resolution and frame rate⁵⁰. The spectral and temperature range are directly related because the peak wavelength of the thermal radiation is inversely proportional to the temperature (Wien’s displacement law). The operating conditions may also influence the choice of spectral range, which can be chosen to avoid radiations from the sun or fit a particular transparency window. As with common digital cameras, the spatial resolution of an infrared camera primarily depends on detector size, lens system and object to camera distance. A typical spatial resolution value for a megapixel infrared camera with a standard 30 mm lens at 3 m distance is 0.8 mm. Temperature resolution is defined as the smallest difference in temperature which can be measured, hence it is dependent on the noise level of the infrared camera over the spectral range. Due to the nonlinear relation between the temperature of an object and the infrared radiation intensity measured by the infrared camera, the temperature resolution is not uniform over the temperature range. Typical values for modern uncooled micro-bolometer focal plane arrays are around 0.02 K at room temperature. It is worth noting that there exists a trade-off between temperature resolution and spatial resolution via the size of the detecting element. On one hand, the sensitivity of the detecting element increases with its size as it collects more flux, but on the other hand, its spatial resolution reduces as its field of view widens. Typical frame rate values of megapixel infrared cameras lie in the range 30 -100 Hz, and the frame rate increases with lower number of pixels.

Thermography is efficiently used as a qualitative tool by showing temperature differences which may indicate leaks or defaults in an object. It can also be used as a quantitative tool but then requires careful calibration to a specific application in order to provide accurate temperature measurements. The main limitation of the temperature accuracy of thermal imaging is that no real object behaves as an ideal blackbody and hence the emission of thermal radiation from different objects at the same temperature may differ significantly. For example, glass and metal at the same temperature will actually look very different with an infrared camera, which translates into large differences in their emissivity values. Another source of error comes from reflected or transmitted infrared radiation, which may compete with emitted thermal radiation, especially for objects with low emissivity.

Thermography techniques are generally classified into two main categories, passive and active. Passive thermography images the temperature of objects without any external heat stimulation as the objects themselves act as heat sources. In active thermography, heat is provided to the objects in order to generate temperature contrasts. Various heat stimulation methods can be employed to image the response of the object, such as pulsed thermography⁵¹, lock-in thermography⁵² or pulsed phase thermography⁵³. The heating mechanism itself can be as diverse

as eddy current induction, ultrasonic vibrations, microwave dielectric heating⁵⁴ or flash lamp heating⁵². Passive thermography is used in medical sciences⁵⁵, surveillance and condition monitoring⁵⁶, while active thermography is used for defect detection^{51,52}, material characterization and measurement of coating thickness.

Bison et al. employed lock-in thermography to detect a localized loss of material through a metallic plate⁵². They applied a uniform modulated heat flux to the undamaged surface of the plate with two lamps and recorded temperature maps of the surface at regular intervals. From a sequence of temperature maps, they recovered the amplitude and phase of the oscillating temperatures for each pixel. The phase image then clearly revealed the damage on the metallic plate. In another study⁵¹, Jönsson et al. applied pulsed thermography with flash lamps for the evaluation of corrosion on carbon steel and magnesium. They used a cooled infrared camera with a spectral range of 3.0 – 5.0 μm , a resolution of 640 px x 512 px, a frame rate of 126 Hz, and a flash lamp consuming 6 kJ for 1 ms to generate short pulses. They demonstrated the superior performance of the method at detecting blisters and filiform corrosion under coatings thicker than 60 μm , compared to three-dimensional profilometry with a photometric stereo technique. Pulsed phase thermography has been applied by Schönberger et al. to investigate the corrosion of steel and galvanized steel coated with organic paints propagating from stone chipping defects⁵³. They identified corrosion spots on 100 x 200 square centimetres surfaces using a cooled infrared camera with a spectral range of 3.0 – 5.0 μm , a resolution of 640 px x 512 px and a frame rate of 100 Hz, combined with xenon lamps delivering approximately 6 kJ of energy in form of a short square pulse. By using high-resolution infrared imaging with a microscope objective, pulsed phase tomography could even differentiate corrosion attack, delamination, uncoated areas and intact areas on surfaces smaller than 10 x 10 square millimetres.

Infrared thermography systems are already commonly mounted on drones for applications such as building inspection, security and rescue, power line monitoring, etc. However, these systems employ passive thermography techniques which are suitable for defect detection under specific conditions only. For example, passive thermography methods have been applied to the detection of delamination on reinforced concrete structures, using the evolution of the outdoor ambient heat due to day-night cycle as a 24 hours sinusoidal heating mechanism. Air gaps have lower thermal conductivity than concrete and are revealed by the thermal amplitude variation over the course of a day. Active thermography is a more versatile technique for defect detection as it can be applied to a wider range of materials and ambient conditions. However, it requires additional equipment, which drains the drone resources (payload, battery capacity) and raises technical challenges such as drone position stability during the measurement. Pulsed thermography and pulsed phase thermography require a high energy pulse of a few kilojoules for each thermal image therefore the surface that can be imaged by a drone-mounted thermography system gets rapidly limited by the battery capacity of the drone. Nevertheless, both pulsed thermography techniques remain viable by allowing quick measurements (< 1 s) under a large variety of ambient conditions, which match the requirements of drone-based sensors. On the other hand, lock-in thermography requires longer measurement times and may suffer high noise due to instability of the drone position, which does not make it a suitable method for drone applications.

2.4 Fourier-transform infrared spectroscopy (FTIR) / Mid-Infrared spectroscopy (MIR)

Infrared (IR) spectroscopy measures the absorption of a sample over a wide spectral range as the absorption of IR light directly reflects molecular bonds in the sample and can provide

complementary information about these to elemental analysis methods such as e.g. inductively coupled plasma mass spectrometry or X-ray fluorescence spectroscopy. The IR electromagnetic spectrum is usually divided into three regions; the near-infrared (NIR) covers approximately $14000 - 4000 \text{ cm}^{-1}$, the mid-infrared (MIR) $4000 - 400 \text{ cm}^{-1}$ and the far-infrared (FIR) $400 - 10 \text{ cm}^{-1}$.

In the simplest implementation of IR spectroscopy, the spectrum is recorded by using a dispersive optical element to split the light transmitted or reflected from the sample into different wavelengths. However, depending on the wavelength region, IR spectroscopy possesses a number of challenges. The ambient air or the used optical components might not be transparent for the light used. Thus, the optical components and the wavelength region needs to be chosen carefully. The main advantage of IR spectroscopy and especially MIR spectroscopy are the possibility to acquire abundant information in organic molecules about functional groups and possible quantitative measurements.

Classical approaches of IR spectroscopy have been used to study atmospheric corrosion and corrosion products in the lab^{57,58}. Raman et al. were able to distinguish and identify rust phases in different samples and their transformation under heat. Misawa et al. studied a similar problem on low alloy steel⁵⁹. Both groups confirm their findings with alternative methods. Moreover, the use of dispersive IR spectroscopy in corrosion science has been sparse in favour of FTIR and Raman spectroscopy, due to their easier use in the laboratory. Zeylikovich and coworkers investigated the wavelength-dependent transmission of paint and found transmission windows for military paint between $1 \mu\text{m}$ and $2.8 \mu\text{m}$, and between $3.8 \mu\text{m}$ and $5.5 \mu\text{m}$ ⁶⁰. Their method showed promising results and was patented^{61,62}. It formed the basis for the CUPID system for imaging through paint⁶¹. The system demonstrated promising results in imaging corrosion damages under paint layers, but since the system is highly dependent on the paint used, it has not been brought to wide usage and the relevance of the approach for a flexible system is limited.

Fourier-transform infrared spectroscopy (FTIR) utilizes light with typical photon wavenumber within the MIR region, between 600 cm^{-1} and 4000 cm^{-1} . While most other spectroscopic methods use a dispersive spectrometer to directly measure the spectral density of the transmitted or reflected light, FTIR relies on an indirect acquisition technique. A broadband infrared light source is filtered by a Michelson-Morley interferometer and the spectral response of the sample to the light from the output port of the spectrometer is recorded depending on the path difference of the two interferometer arms. By applying a Fourier-transformation to the raw data the actual spectrum is obtained. FTIR analysis enables fast (typically 10 - 100 spectra/sec)^{63,64} identification of polymers, non-metallic materials, mineral compounds and organic molecules and covers the fundamental vibrational modes of anion functional groups such as SiO_4 , CO_3 , PO_4 , and SO_4 ⁶⁵. This technique was used to examine the corrosion process of steel components in a printing machine, where the spectra revealed corrosion products of steel and enabled identification of iron oxides including goethite ($\alpha\text{-FeO(OH)}$), lepidocrocite ($\gamma\text{-FeO(OH)}$) and magnetite (Fe_3O_4)⁶⁶. Quantitative studies of iron oxides were also approached systematically by using FTIR in magnetite (Fe_3O_4), maghemite ($\gamma\text{-Fe}_2\text{O}_3$), and hematite ($\alpha\text{-Fe}_2\text{O}_3$)⁶⁷. When studying heritage materials, some inorganic pigments containing iron oxides are inactive in the MIR region but display resonances in the FIR region which have been successfully probed by FTIR on mural paintings and corrosion products in printers^{68,69}.

FTIR and Raman spectroscopy are complementary analytical methods that both probe the intrinsic vibrational modes of molecular bonds but obey different selection rules. However, FTIR generally provides better sensitivity than Raman spectroscopy and a comparable capability to identify minerals. In addition, the IR bands can exhibit measurable band shifts with cation

substitution that provide information required for mineral identification. Besides, carbon dioxide (CO₂), which is found in oil and gas fields in varying concentrations, can cause severe corrosion of infrastructures in the presence of water. FTIR is sensitive to the detection of CO₂ and may therefore be employed as a corrosion prevention tool.

The deployment of an IR spectrometer on a drone has been demonstrated by T&A Survey Drone Services in the Netherlands for mining-related environmental monitoring and crop monitoring, where it has provided detailed spectral information of soil, rocks and vegetation⁷⁰. The specificity and the availability of alternative methods can explain why dispersive IR spectroscopy is not used widely for corrosion analysis. However, the relatively simple setup and the possibility to integrate it on a drone make it promising and incite further investigation.

Integration of the components needed for the system of Alfano et al.⁶¹ onto a drone has already been shown. IR cameras in the relevant wavelength range are available for deployment on a drone and the additional power consumption and weight of an IR light source is in a compatible range.

However, there are multiple concerns in integrating specifically an FTIR spectrometer on a UAV platform. Since this technique relies on the precise control of the position of a mirror and on the stability of two interferometric arms, the vibrations on a drone may cause excessively noisy measurements. Besides, most FTIR instruments are laboratory instruments. Typical weights for in field remote imaging instruments are around 33 kg, which is too heavy for drone deployment and makes this technique not very favourable⁷¹.

2.5 Colour, multispectral, and hyperspectral imaging and VIS-NIR spectroscopy

Colour imaging, multispectral imaging and hyperspectral imaging are all detection methods of the visible part of the electromagnetic spectrum. Multi- and hyperspectral imaging and VIS-NIR spectroscopy are normally also sensitive in the NIR region. They differ mainly in the spectral resolution, number of bands, acquisition time and cost.

The corrosion detection techniques relying on imaging presented in this section are inherently not quantitative and still require human comparison and rating. However, recent efforts have aimed at overcoming these drawbacks by applying machine learning algorithms and artificial intelligence. Current results are discussed in the last part of this section.

2.5.1 Colour imaging

Colour imaging relies on the acquisition of images that mimic the spectral perception of the human eye. The images are formed by recording the intensity of radiations in three overlapping bands: the red band from 575 nm to 650 nm, the green band from 475 nm to 600 nm and the blue band from 400 nm to 525 nm. The most common practice to image in these three bands simultaneously is by covering the imaging sensor with a Bayer filter. This regular filter pattern lets the green part of the spectrum to half of the pixels, while the green and blue part of the spectrum is imaged on one quarter of the pixels each. An interpolation algorithm reconstructs the full colour information after acquisition for all pixels. NIR light is blocked by a filter, since the human eye is not sensitive to these wavelengths and would cause an overexposed perception of the image.

An advantage of this technique is the natural resemblance of the sample, allowing the inspector to easily evaluate the sample from the acquired image or validate results from a different method. Moreover, cameras of different price categories are available and carrying a high performance camera on a drone represents the main analytic technique. Since they are inherently not chemically sensitive, the detection of corrosion relies on the perception of colour with its

restrictions and the requirement of an inspector. Advanced analysis techniques and their performance are discussed below.

2.5.2 Multispectral imaging

Multispectral imaging is often combined with colour imaging to record images in the NIR region or in specific narrower wavelength bands. In comparison with colour imaging, a wider variety of imaging sensors can be used for multispectral imaging depending on requirements for size, cost, covered spectral bands and frame rate, while the covered wavelength range can span from about 300 nm to 1100 nm and the choice of spectral bands is only limited by the availability of optical bandpass filters. Modern manufacturing techniques allow the production of filters over the whole spectrum. Bandwidths can be customized from a few nanometres up to tens of nanometres. Multispectral imaging is commonly used with drones for the recording of the vegetation index in farming. Therefore, sensors for drone deployment are already available and would only have to be adapted for the required wavelengths to detect corrosion. Unfortunately, corrosion products do not exhibit clear absorption lines as such. This makes the detection method relatively cheap and deployable but the advantage over colour imaging is limited. More details about this issue are discussed in the subsection on VIS-NIR spectroscopy.

2.5.3 Hyperspectral imaging

Hyperspectral imaging is implemented by mounting a narrow tuneable bandpass filter in front of a monochrome camera and taking multiple pictures of the same sample in rapid repetition, while adjusting the pass wavelength of the filter in between the images. The amount of recorded data is usually significantly greater than with colour or multispectral imaging as the number of spectral bands covered by a hyperspectral image is higher. In order to reduce the amount of collected data and increase the amount of light per pixel, many hyperspectral cameras operate with relatively low resolution sensors.

Both multi- and hyperspectral-imaging are generally not used for the detection of corrosion. The main reason is the limited advantage of the technique over colour imaging, due to the lack of significant absorption and emission lines in iron oxides that could be used as fingerprints. However, the spectral response of iron oxides have been used in mineralogical characterization of gleys⁷² and determination of the mixture ratio of iron oxides⁷³. Both studies concluded, that the technique is able to identify the different iron oxides in most cases⁷³. However, the studies limited the analysis to predefined samples of iron oxide containing powders, gleys and the oxides themselves. These samples are considerably less complex than the samples considered in corrosion inspection, where a mixture of different iron oxides, coating and other organic materials present in the environment will complicate the measurement. This makes a transition to corrosion detection challenging.

2.5.4 VIS-NIR spectroscopy

Near-infrared (NIR) spectroscopy is a spectroscopic technique using the electromagnetic spectrum from about 700 nm to 2500 nm to probe the molecular and atomic bands of a material. This section will focus only on wavelengths below 1100 nm, which address electronic transitions, while the section about FTIR and MIR spectroscopy covered longer wavelengths, which address molecular transitions. VIS-NIR spectroscopy also covers the visible range from 300 nm to 700 nm. This section will focus on active spectroscopic techniques, which require an artificial light source, while colour, multi- and hyperspectral imaging rely on the presence of ambient light.

The reflectance spectra and their associated electronic spectra of iron oxides have been studied extensively, e.g. by Scheinost et al.⁷⁴, Sherman and Waite⁷⁵ or Torrent and Barron⁷³. They report four distinct bands in all iron oxides at about 410 nm, 480 nm, 700 nm and 950 nm with the exception of hematite. The absorption bands in hematite are at around 420 nm, 532 nm, 700 nm and 875 nm.

On a technical side, the absorption bands are wide without sharp features, thus do not require high-resolution spectroscopy and can be probed with a wideband light source. Implementing this technique by coupling a light source with hyperspectral imaging on a drone seems feasible and sufficient in terms of resolution.

Scheinost et al.⁷⁴ studied the reflectance of iron oxide minerals and found significant differences in the position and intensity of the bands, for the same type of material in different samples. They account these onto differences of crystal structure. The magnitude of the position shifts can lead to band overlaps, complicating a distinct identification of materials. Despite these problems, VIS-NIR spectroscopy has found some very specific applications in identification and quantification of iron oxides in soil samples^{76,77} and in the paper industry⁷⁸. Due to the unspecific identification scheme, this technique does not offer any advantages over normal colour imaging or visual inspection. Industry has not implemented it for corrosion detection and is relying on photographs and contact inspection.

2.5.5 Advanced analytical data evaluation

Multiple advanced analytics approaches have been developed to overcome the need for a human corrosion specialist to evaluate the state of corrosion. Colour images have been analysed using a colour-based digital imaging processing approach⁹. This approach analysed the pixel values in terms of the HSV colour model (hue, saturation, value). By determining a certain colour range as corrosion, the algorithm was able to classify up to 27 rust grades, while the accuracy when used on the sample pictures in ASTM D610¹¹ was determined to 0.01 to 0.02. Although the procedure would fulfil most of the requirements, the detection is not specific to corrosion products. Moreover, it would require assistance for image adjustment, detection of unusual shapes and distinction of materials with similar colours.

Momma et al.⁷⁹ used colour images of rust on steel structures to train and test a support vector machine for corrosion recognition and they achieved a correct classification of 66% of their images. Petricca and coworkers⁸⁰ used pixel wise colour pre-categorization and deep learning algorithms for detection of corrosion in colour images. Notably, their aim is to use their technology for drone-based inspection. Their pre-categorization of images with OpenCV achieved an accuracy of 69% and their deep learning approach of 78%, while both methods combined allowed for accuracies of up to 88%.

Huynh et al.⁸¹ employed hyperspectral cameras to evaluate the condition of the Sydney Harbour Bridge. They acquired spectral images in the range 450 nm to 650 nm, which provides an increase in spectral resolution while preserving the same sensing bandwidth compared to RGB cameras. Their approach of supervised learning of a multi-class support vector machine allowed them to automatically detect corroded subareas within their pictures and classify them in four degradation and one background categories according to the different ASTM standard classes. They achieve correct classification rates of between 75% and 85% depending on the level of degradation present.

Overall most of the advanced analytical methods are currently not able to deliver our required uncertainty level below 5%. Classifying the images based on the position of the pixels in colour

space seems promising but the method needs to prove its performance in more challenging conditions.

2.5.6 Overall conclusion

Colour and hyperspectral imaging systems are a typical load on drones. By themselves, the recorded images do not provide sufficient information for the specific identification and automatic evaluation of the corrosion state of an asset. While manual rating from colour images is a widely accepted approach, it heavily relies on the inspector and its objectivity. Advanced computational approaches to analyse recorded images lack currently the necessary accuracy for their wide spread use in corrosion evaluation applications.

2.6 Raman spectroscopy

Raman spectroscopy relies on the inelastic scattering of a monochromatic laser beam from a sample. Excitation or deexcitation of molecular vibrations lead to a shift in frequency of the reemitted photons. Since the energy shift is caused by the characteristic molecular levels of the molecules under investigation, the spectrum of the scattered photons acts as a fingerprint⁸².

Raman scattering is an inherently weak process with typical scattering rates on the order of 1 in 10 million⁸³. Moreover it is an omnidirectional process, which complicates the efficient collection of the scattered photons. The strong absorption of iron oxides⁸⁴ also contributes to the lowering of the signal obtained from corrosion products, which renders the evaluation of corrosion with Raman scattering particularly challenging.

Nonetheless, Raman spectroscopy is one of the standard tools to identify corrosion products on different types of steel due to their distinctive spectra. It proved to be especially useful, when combined with microscopic imaging⁸⁵. However, most studies have been performed in a controlled laboratory environment, allowing for near-contact probe-sample distances, high numerical aperture collection optics and long exposure times, which are not feasible conditions when measuring from a flying drone platform^{85–87}.

By choosing the wavelength of the excitation laser close to an electronic transition in the examined material, the amount of scattered photons can be increased by a factor of 10^2 to 10^6 ⁸⁸. This scattering enhancement process called resonance Raman scattering has been demonstrated to work in iron oxides for excitation wavelengths of about 532 nm⁸⁹ and 636 nm⁸⁷. These results have been reproduced in laboratory conditions at DFM. However, the achieved enhancement was not large enough to allow for remote detection of iron oxides within acceptable timeframes. Moreover, we anticipate the presence of titanium dioxide (TiO_2) in real life samples, since it is widely used as a white pigment in protective paints⁹⁰. The strong Raman spectrum of titanium dioxide overlaps with the weak spectra of iron oxides, potentially masking the presence of corrosion⁹¹. In conclusion, the use of Raman spectroscopy for detection of corrosion from drones is not favourable without dramatic improvements of Raman spectroscopy methods for iron oxides.

2.7 Laser-induced breakdown spectroscopy (LIBS)

Laser-induced breakdown spectroscopy (LIBS) is an elemental analysis technique considered non-destructive (or minimally destructive) and requiring short high-intensity pulse lasers, as well as virtually no sample preparation. LIBS is an atomic emission spectroscopy technique, which involves the creation of a high-temperature plasma at the surface of the sample by ablation of a small amount of material with a high intensity focused laser pulse. During the process of plasma cooling, which happens about 10 μs after the laser pulse excitation, the electrons of the atoms and ions in excited electronic states fall down into their ground states. This causes the plasma to

emit light at characteristic atomic emission lines enabling the identification of the elements in the sample.

Technically, LIBS consists of a high-energy nanosecond pulse laser and a spectrometer with a high-sensitivity, time-gated detector. Nearly all elements have emission lines within conventional silicon CCD spectral response (300 - 1100 nm), which allow for the utilization of cheap and widely used spectrometer technology. The spectral resolution of the spectrometer is an important factor for the differentiation and identification of the elements of a sample. For example, Fe has emission lines (248.3 nm, 407.2 nm) close within 0.6 nm to emission lines of C (247.8 nm) and Sr (407.8 nm). LIBS measurements are also subject to variations in laser intensity at the sample and resultant energy of the plasma, which limits their reproducibility. However, with appropriate calibration prior to measurements, the accuracy can still be kept below 5%, and the sensitivity under 1 ppm by mass⁹².

LIBS has inherent standoff detection capability because of the relatively intense light emission from the plasma. Rohwetter et al. have demonstrated LIBS on metallic targets at distances up to 180 m⁹³. They used filaments produced by femtosecond and terawatt laser pulses to propagate optical beams with submillimetre diameters over long distances. A more practical example for drone deployment is the ChemCam instrument mounted on the Curiosity Mars Rover, which performs LIBS measurements from distances up to 7 meter⁹⁴.

In addition to remote LIBS systems, there exists handheld LIBS instruments, which are so far mostly applied to scrap metal sorting, quality assurance in metal fabrication and alloy analysis in general. However, these handheld instruments require contact with the sample for accurate measurements, which makes them unsuitable for remote detection of corrosion degradation.

LIBS is a powerful technique for rapid, real-time elemental analysis of a wide range of materials, from metal and gemmological samples to chemical and biological agents. It has been extensively used for the identification of minerals and rocks, which include iron oxides⁹². With regard to corrosion, LIBS has been essentially applied to the study of oxidation layers on archaeological artefacts⁹⁵. It enables depth profiling of the corrosion layers by “drilling” through materials via laser ablation.

Although LIBS is commonly used for production control and quality assurance in metal industries and has been demonstrated to provide qualitative and quantitative information on corrosion products in archaeological sciences, there is nearly no report of application of LIBS as a test and evaluation method for corrosion degradation.

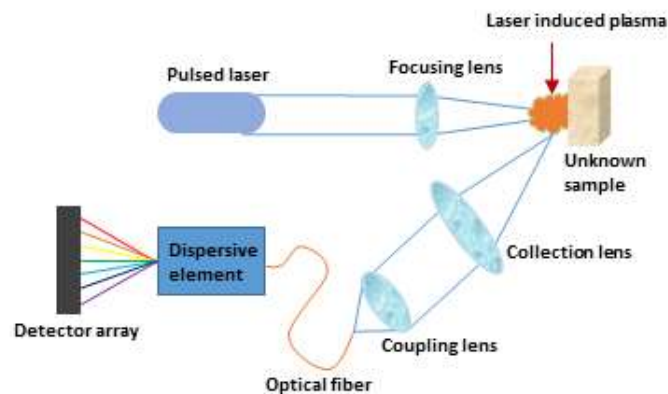


Figure 1 Illustration of a laser-induced breakdown spectroscopy setup

2.8 X-ray spectroscopy

X-ray spectroscopy is an elemental analysis technique, which includes several distinct methods employing X-radiation, such as X-ray absorption spectroscopy (XAS), X-ray emission spectroscopy (XES) and X-ray diffraction (XRD).

X-ray spectroscopy methods rely on the excitation or ejection of core electrons in a material by high-energy X-ray photons. This process involves the absorption of all (X-ray absorption) or part (X-ray Raman scattering) of the X-ray photon energy. The resulting unstable excited state relaxes by releasing energy in the form of an X-ray photon (X-ray fluorescence) or an Auger electron. The excitation and relaxation energies depend on the electronic structure of the material and thus constitute a fingerprint of the material.

XRD provides information on the atomic and molecular structure of crystalline materials by observing the interference patterns resulting from the elastic scattering of X-rays on crystal planes.

Technically, XAS is more demanding than XES and XRD as it requires a tuneable X-ray source, which is usually a synchrotron radiation source. There are currently no available portable synchrotron radiation sources, which prevents the application of XAS in the field. In comparison, XES and XRD typically uses high-energy X-ray beams generated by X-ray tubes, which can be implemented into compact instruments.

From the detection side, XRD employs gas or semiconductor X-ray detectors but also mechanical adjustment of the angle of the incident X-ray beam onto the sample and of the angle of detection of diffracted X-ray radiations having a direct influence onto the mechanical feasibility for integrating the measurement technology onto a drone. Furthermore XRD usually requires sample preparation by grinding a small amount of material into a powder, thus do not apply for non-destructive remote sensing. These technical limitations have prevented the development of handheld XRD instrument but portable XRD instruments of the size of a small briefcase and weighting less than 15 kg have been developed for field measurements⁹⁶.

Concerning XES, handheld instruments based on X-ray fluorescence (XRF) are commercially available and enable qualitative and semi-quantitative measurements of the elemental composition of a wide range of materials for applications in mining, metal and alloy industries, art conservation, jewellery, etc. XRF detection requires the use of an energy-dispersive X-ray (EDX) spectrometer or a wavelength-dispersive X-ray (WDX) spectrometer. The former counts the X-ray photons according to their energy and the later to their wavelength. WDX spectrometers provide a finer spectral resolution than EDX spectrometers but require longer acquisition times as they employ a scanning monochromator for separating photons at different wavelengths and acquiring a spectrum. Therefore, most handheld XRF instruments are built with EDX spectrometers.

Sarrazin et al. have demonstrated a portable XRD-XRF instrument requiring no sample preparation for non-invasive and non-contact study of art objects⁹⁷. Originally designed for the analysis of the chemistry and mineralogy of Martian soil⁹⁸, Sarrazin and co-workers developed the technology further for the in-field use for geology and for the non-contact analysis of artwork. Due to the powder diffraction method the instrument still requires near-contact operation and is limited to the study of finely grained materials such as dyes in paints. The non-contact XRD-XRF instrument was commercialized by inXitu but is no more available since Olympus bought the company⁹⁹. The portable XRD-XRF instrument for in-field measurements is still available from Olympus under the name TERRA Portable XRD. According to the manufacturer, the instrument is capable of identifying and quantifying the different corrosion products by characterizing their crystallographic structure¹⁰⁰.

Handheld XRF instruments are used in the inspection of piping systems for preventing sulfidic corrosion¹⁰¹. In this application, XRF analyses the content of silicon in carbon steel, which indicates the risk of sulfidation corrosion. In general, XRF can detect corrosion indicative elements in metal alloys, such as Si, Cr, Ni, and Cu, but cannot identify the corrosion products themselves. Corrosion detection can also be performed by X-ray inspection (XRI), which is based on projectional X-ray radiography where a beam of high-energy photons is sent through the object under inspection and collected on the other side of the object. The loss of photons through the object depends on the density of its constituent materials, thus the obtained radiography image indicates density variations which may be attributed to corrosion, welds, wet insulation, etc. XRI enables imaging through insulation and paint layers but requires access to two opposite sides of the inspected object, thus it is essentially used for inspection of metal pipes with an insulating layer.

Finally yet importantly, care must be taken when using X-ray radiations, as they can be harmful and legal restrictions apply. X-ray instruments may require heavy shielding which limits their applicability on a drone platform. All these aspects make X-ray spectroscopy either impossible or at least unfavourable to realize on a drone depending on the specific method used.

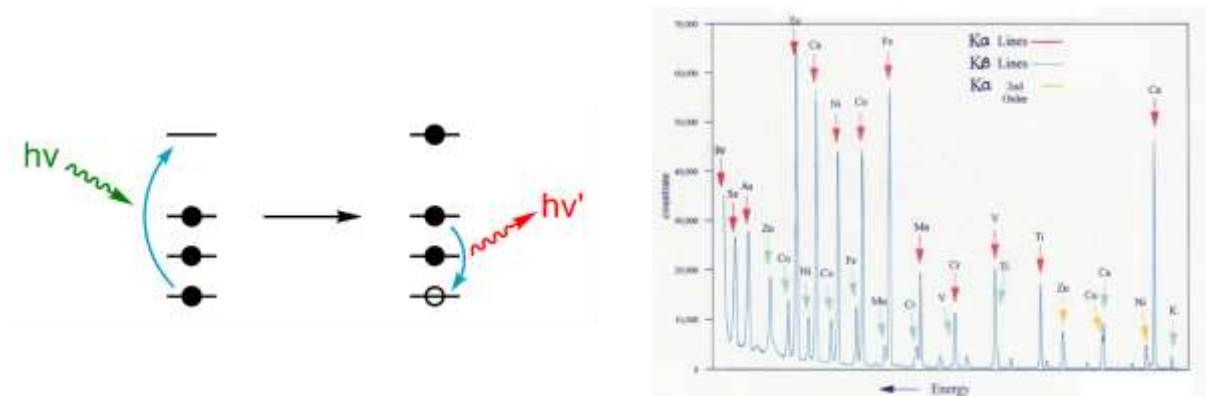


Figure 2 (Left) Illustration of the XRF principle¹⁰². (Right) Example of an XRF spectrum¹⁰³.

3. Evaluation and conclusion

Many different methods have been investigated for detecting and evaluating corrosion degradation but few have so far reached or have the potential to reach a stage of development sufficient for being deployed efficiently on drones.

Methods such as THz spectroscopy and microwave imaging are promising for the detection of corrosion damages under paints and coatings but measurement constraints, like short probe-target distance and position stability, prevent their practical deployment on a drone. On the other hand, simple and fast imaging methods with a RGB, hyperspectral or multispectral camera, are easily applicable with drones but are limited to the analysis of the surface of the samples, and thus cannot be applied to the early detection of corrosion under paints and coatings, or inside concrete structures. Nevertheless, they are promising tools when combined with advanced data analysis methods involving machine learning algorithms. In theory, a computer trained with sufficient data and provided with enough information should provide a more objective rating of surface deterioration from camera images than a human inspector could.

Measurement methods like Raman spectroscopy, FTIR spectroscopy, dispersive IR spectroscopy and LIBS reveal chemically specific information about the sample, which enables the identification of corrosion products and their differentiation from coatings and paints. Furthermore, the technology itself allows for detection across distances of several meters. As promising as it sounds, these methods however face important practical limitations due to their poor imaging capabilities over large surface areas. Moreover, Raman spectroscopy applied to the identification of corrosion products requires single-point acquisition times of several minutes, which are too long for drone deployment.

Among the most promising techniques for corrosion degradation detection on drones figure multispectral imaging and infrared thermography. One of their major advantages is that both methods are already commonly used for drone applications. However, the two techniques have different imaging capabilities. Multispectral imaging enables coarse material identification by measuring the reflectance spectra of surfaces, whereas infrared thermography can image through a few centimetres inside the sample and detect hidden defects but cannot identify corrosion products. In order to enlarge the range of applications for infrared thermography with drones, it would be advantageous to develop active thermography system for drone deployment, which has not been done before to our knowledge.

Method	Corrosion degradation sensing capability	Drone compatibility (payload)	Drone compatibility (technical)	Overall rating
Microwave spectroscopy	Good Sensitive to swelling and blistering. Coarse material differentiation capabilities by spectral imaging. Can image through a few centimetres of paints, coatings and concrete.	Good Microwave radar systems have been deployed on drones for geomatic surveys.	Poor Short sensing distance. Probe positioning requirements do not match noisy drone environment.	Poor
THz spectroscopy	Good Sensitive to swelling and blistering, roughness and probably to oxide products. Can image through a few centimetres of paints, coatings and concrete.	Good Demonstrated with a gas measurement system deployed on a drone.	Poor Short sensing distance. Probe positioning requirements do not match noisy drone environment.	Poor
Infrared thermography	Good Sensitive to swelling and blistering. Coarse material differentiation capabilities.	Fair Passive thermography instruments have already been deployed on drones.	Fair Large field of view imaging but lower resolution than conventional cameras.	Good

	Can image through a few centimetres of paints, coatings and concrete.	Active thermography uses heating sources that may drain the drone battery.		
FTIR	Fair Measure molecular composition, can identify corrosion products. Slightly higher sensitivity to corrosion products than Raman spectroscopy. Limited to surface detection, cannot image through materials.	Poor No handheld commercial systems available. Sturdy mount to hold interferometer stable is needed.	Fair Point sensing operation limits imaging of large surface areas.	Poor
IR spectroscopy	Fair Measure molecular composition, can identify corrosion products. Slightly higher sensitivity to corrosion products than Raman spectroscopy. Can image through specific coatings.	Good Commercially available compact handheld spectrometers.	Fair Point sensing operation limits imaging of large surface areas.	Fair
VIS-NIR spectroscopy	Fair Similar to camera techniques. Specificity to corrosion products is limited by the lack of characteristic absorption and emission lines in iron oxides.	Good Commercially available compact handheld spectrometers.	Fair Point sensing operation limits imaging of large surface areas.	Fair
RGB camera	Fair Low specificity to corrosion products. Require human inspector or machine learning methods for differentiating corrosion damages. Limited to surface detection, cannot image through materials.	Excellent Standard sensor on almost all drones.	Excellent Large field of view imaging and cheap.	Fair

Multispectral camera	Fair Similar to RGB camera with slightly higher specificity to corrosion products.	Excellent Commercially available multispectral imaging system for drone deployment	Excellent Similar to RGB camera but more expensive.	Good
Hyperspectral camera	Fair Similar to multispectral camera. Specificity to corrosion products is limited by the lack of characteristic absorption and emission lines in iron oxides.	Excellent Commercially available multispectral imaging system for drone deployment	Good Large amount of data necessitates high-capacity storage onboard or fast communication to ground.	Fair
Raman spectroscopy	Poor Measure molecular composition, can identify corrosion products. Low sensitivity to corrosion products. Limited to surface detection, cannot image through materials.	Good Commercially available compact handheld Raman spectrometers	Poor Long acquisition times (several minutes). Restrictive safety regulations over unshielded high power laser light.	Poor
Laser-induced breakdown spectroscopy (LIBS)	Fair Measure elemental composition, can identify corrosion products. Enable depth profiling of corrosion layers by laser ablation through materials.	Good A compact LIBS system has been deployed on the Mars rover Curiosity	Fair Point sensing operation limits imaging of large surface areas. Restrictive safety regulations over unshielded laser light.	Fair
X-ray spectroscopy	Good XRF can measure elemental composition, and XRD can identify corrosion products. Both are limited to surface detection and cannot image through materials. XRI can image through materials and detect hidden defects.	Fair Handheld XRF and portable XRD and XRI systems commercially available.	Poor (Near-) contact and point sensing operation of XRF and XRD. Restrictive safety regulations over unshielded X-ray radiations.	Poor

Table 2 Overview of the discussed techniques and their performance and viability.

4. Bibliography

1. Koch G, Varney J, Thompson N, Moghissi O, Gould M, P. J. *International Measures of Prevention, Application, and Economics of Corrosion Technologies Study*. (NACE International, 2016).
2. Bygnings- og Boligministeriet Transport. Bekendtgørelse om flyvning med droner i bymæssigt område. *BEK nr 1256* (2017).
3. Bygnings- og Boligministeriet Transport. Bekendtgørelse om flyvning med droner uden for bymæssigt område. *BEK nr 788* (2017).
4. DJI. Datasheet DJI Matrice 600. (2017).
5. Eva-Carina Nørskov, Jesper Villadsen, Niels Berg Conradsen, S. Y. S. Kortlægning af droner i Danmark. *Teknol. Inst.* (2016).
6. Hald, J. RK Dronemetrologi. *Bedreinnovation.dk* (2017).
7. DJI. Datasheet A3 flight control system. (2017).
8. DJI. Datasheet Ronin-M. (2017).
9. A.W.Momber. Quantitative performance assessment of corrosion protection systems for offshore wind power transmission platforms. *Renew. Energy* **94**, (2016).
10. EN ISO 4628-3:2016. *Paint. Varn. Degrad. coatings—Designation Quant. size defects, intensity Unif. Chang. Appear. Part 3 Assess. degree rusting 1*, (2016).
11. ASTM. ASTM D 610. *ASTM D 610- SSPC Vis 2* (2001).
12. D'imprimerie, C. E. des associations de fabricants de peintures et d'encres. 'European scale of degree of rusting for anticorrosive paints'. (1964).
13. GL, D. Corrosion protection of ship. *DNVGL-CG-0288* (2017).
14. Kharkovsky, S., Ryley, A. C., Stephen, V. & Zoughi, R. Dual-Polarized Near-Field Microwave Reflectometer for Noninvasive Inspection of Carbon Fiber Reinforced Polymer-Strengthened Structures. *IEEE Trans. Instrum. Meas.* **57**, 168–175 (2008).
15. Miszczyk, A. & Darowicki, K. Inspection of protective linings using microwave spectroscopy combined with chemometric methods. *Corros. Sci.* **64**, 234–242 (2012).
16. Kharkovsky, S. & Zoughi, R. Microwave and millimeter wave nondestructive testing and evaluation - Overview and recent advances. *IEEE Instrum. Meas. Mag.* **10**, 26–38 (2007).
17. Li, C., Tofighi, M.-R., Schreurs, D. & Horng, J. T.-S. *Principles and Applications of RF/Microwave in Healthcare and Biosensing*. (2016).
18. Sheen, D. M., McMakin, D. L. & Hall, T. E. Three-dimensional millimeter-wave imaging for concealed weapon detection. *IEEE Trans. Microw. Theory Tech.* **49**, 1581–1592 (2001).
19. Kharkovsky, S. *et al.* Application of microwave 3D SAR imaging technique for evaluation of corrosion in steel rebars embedded in cement-based structures. in *AIP Conference Proceedings* 1516–1523 (2012). doi:10.1063/1.4716395
20. Hong Zhang, Y. H. *et al.* Evaluation of Atmospheric Corrosion on Coated Steel Using K - Band Sweep Frequency Microwave Imaging. *IEEE Sens. J.* **16**, (2016).
21. Ghasr, M. T., Carroll, B., Kharkovsky, S., Austin, R. & Zoughi, R. Millimeter-Wave Differential Probe for Nondestructive Detection of Corrosion Precursor Pitting. *IEEE Trans. Instrum. Meas.* **55**, 1620–1627 (2006).
22. ITU-R. Objective quality coverage assessment of digital terrestrial television broadcasting signals of Systems A and B. *BT Ser. Broadcast. Serv.* (2012).
23. Ahi, K. & Anwar, M. Advanced terahertz techniques for quality control and counterfeit detection. in *Proc. SPIE 9856 Terahertz Physics, Devices, and Systems X: Advanced Applications in Industry and Defense* (eds. Anwar, M. F., Crowe, T. W. & Manzur, T.) 98560G (2016). doi:10.1117/12.2228684
24. Broadband Frequency Tripler Operational Manual. *Virginia Diodes, Man.* (2016).
25. Terahertz Technologies Lasers, Accessories and Solutions. *Toptica Photonics, Datasheet* (2017).

26. Williams, G. P. High-power terahertz synchrotron sources. *Philos. Trans. R. Soc. A Math. Phys. Eng. Sci.* **362**, 403–414 (2004).
27. Tan, P., Huang, J., Liu, K., Xiong, Y. & Fan, M. Terahertz radiation sources based on free electron lasers and their applications. *Sci. China Inf. Sci.* **55**, 1–15 (2012).
28. Idehara, T. & Sabchevski, S. P. Gyrotrons for High-Power Terahertz Science and Technology at FIR UF. *J. Infrared, Millimeter, Terahertz Waves* **38**, 62–86 (2017).
29. He, W. *et al.* Generation of broadband terahertz radiation using a backward wave oscillator and pseudospark-sourced electron beam. *Appl. Phys. Lett.* **107**, 133501 (2015).
30. Rizzi, B. J., Hesler, J. L., Dossal, H. & Crowe, T. W. Varactor diodes for millimeter and submillimeter wavelengths. in *Michigan Univ., The Third International Symposium on Space Terahertz Technology: Symposium Proceedings* (1992).
31. Kitagawa, S., Suzuki, S. & Asada, M. Wide-Range Varactor-Tuned Terahertz Oscillator Using Resonant Tunneling Diode. *J. Infrared, Millimeter, Terahertz Waves* **35**, 445–450 (2014).
32. Klatt, G. *et al.* Terahertz emission from lateral photo-Dember currents. *Opt. Express* **18**, 4939 (2010).
33. Köhler, R. *et al.* Terahertz semiconductor-heterostructure laser. *Nature* **417**, 156–159 (2002).
34. Scalfari, G. *et al.* THz and sub-THz quantum cascade lasers. *Laser Photonics Rev.* **3**, 45–66 (2009).
35. Lee, A. W. M. *et al.* Real-time terahertz imaging over a standoff distance (> 25 meters). *Appl. Phys. Lett.* **89**, 141125 (2006).
36. Fatholouloumi, S. *et al.* Terahertz quantum cascade lasers operating up to ~ 200 K with optimized oscillator strength and improved injection tunneling. *Opt. Express* **20**, 3866 (2012).
37. Pagies, A., Ducournau, G. & Lampin, J.-F. Low-threshold terahertz molecular laser optically pumped by a quantum cascade laser. *APL Photonics* **1**, 31302 (2016).
38. Ramakrishnan, G. Enhanced terahertz emission from thin film semiconductor/metal interfaces. (TU Delft, 2012).
39. Kawano, Y. & Ishibashi, K. An on-chip near-field terahertz probe and detector. *Nat. Photonics* **2**, 618–621 (2008).
40. Anastasi, R. F. Terahertz NDE for Under Paint Corrosion Detection and Evaluation. in *AIP Conference Proceedings* **820**, 515–522 (AIP, 2006).
41. Madaras, E. I. *et al.* Application of terahertz radiation to the detection of corrosion under the shuttle's thermal protection system. in *AIP Conference Proceedings* **975**, 421–428 (AIP, 2008).
42. Kurabayashi, T., Yodokawa, S. & Kosaka, S. Terahertz imaging through paint layers. in *37th International Conference on Infrared, Millimeter, and Terahertz Waves* 1–2 (IEEE, 2012). doi:10.1109/IRMMW-THz.2012.6380425
43. Anastasi, R. F. & Madaras, E. I. Terahertz NDE for metallic surface roughness evaluation. in *Proc. SPIE 6176, Nondestructive Evaluation and Health Monitoring of Aerospace Materials, Composites, and Civil Infrastructure V*, 61760O (2006). doi:10.1117/12.659463
44. Plusquellic, D. F., Provenzano, V. & Chou, S. G. THz Spectroscopic Study of Iron Oxide Layers within Steel-Reinforced Structural Components. *MRS Proc.* **1296**, mrsf10-1319-o03-10 (2011).
45. Chou, S. G. *et al.* Using Terahertz Waves to Identify the Presence of Goethite via Antiferromagnetic Resonance. *Appl Magn Reson* (2017).
46. Shin G. Chou, Paul E. Stutzman, Shuangzhen Wang, Edward J. Garboczi, William F. Egelhoff, and D. F. P. High-Resolution Terahertz Optical Absorption Study of the Antiferromagnetic Resonance Transition in Hematite (α -Fe₂O₃). *J. Phys. Chem. C* (2012). doi:10.1021/jp3036567
47. The Thz Drone Project. *Bakman Technologies* (2017). Available at: <http://www.bakmantechologies.com/THz-drone-project.php>.

48. Vollmer, M. & Möllmann, K.-P. *Infrared Thermal Imaging: Fundamentals, Research and Applications*. (Wiley-VCH Verlag GmbH & Co. KGaA, 2010). doi:10.1002/9783527630868
49. Rogalski, A., Martyniuk, P. & Kopytko, M. Challenges of small-pixel infrared detectors: a review. *Reports Prog. Phys.* **79**, 46501 (2016).
50. Venkataraman, B. & Raj, B. Performance parameters for thermal imaging systems. *Insight - Non-Destructive Test. Cond. Monit.* **45**, 531–535 (2003).
51. Jönsson, M., Rendahl, B. & Annergren, I. The use of infrared thermography in the corrosion science area. *Mater. Corros.* **61**, 961–965 (2010).
52. Bison, P., Ceseri, M. & Inglese, G. Mapping corrosion of metallic slab by thermography. *J. Phys. Conf. Ser.* **214**, 12073 (2010).
53. Schönberger, A., Virtanen, S., Giese, V., Schröttner, H. & Spießberger, C. Non-destructive detection of corrosion applied to steel and galvanized steel coated with organic paints by the pulsed phase thermography. *Mater. Corros.* **63**, 195–199 (2012).
54. Foudazi, A., Ghasr, M. T. & Donnell, K. M. Characterization of Corroded Reinforced Steel Bars by Active Microwave Thermography. *IEEE Trans. Instrum. Meas.* **64**, 2583–2585 (2015).
55. Lahiri, B. B., Bagavathiappan, S., Jayakumar, T. & Philip, J. Medical applications of infrared thermography: A review. *Infrared Phys. Technol.* **55**, 221–235 (2012).
56. Bagavathiappan, S., Lahiri, B. B., Saravanan, T., Philip, J. & Jayakumar, T. Infrared thermography for condition monitoring – A review. *Infrared Phys. Technol.* **60**, 35–55 (2013).
57. Nasrazadani, S. & Raman, A. The application of infrared spectroscopy to the study of rust systems—II. Study of cation deficiency in magnetite (Fe₃O₄) produced during its transformation to maghemite (γ-Fe₂O₃) and hematite (α-Fe₂O₃). *Corros. Sci.* **34**, 1355–1365 (1993).
58. Raman, A., Kuban, B. & Razvan, A. The application of infrared spectroscopy to the study of atmospheric rust systems—I. Standard spectra and illustrative applications to identify rust phases in natural atmospheric corrosion products. *Corros. Sci.* **32**, 1295–1306 (1991).
59. Misawa, T., Asami, K., Hashimoto, K. & Shimodaira, S. The mechanism of atmospheric rusting and the protective amorphous rust on low alloy steel. *Corros. Sci.* **14**, 279–289 (1974).
60. Zeylikovich, I. *et al.* Mid-IR transmission window for corrosion detection beneath paint. *Electron. Lett.* **39**, 39 (2003).
61. Robert R. Alfano, Iosif Zeylikovich, Wubao Wang, Jamal Ali, Vincent Benischek, Y. B. Systems and methods for non-destructively detecting material abnormalities beneath a coated surface US 6853926 B2. (2005).
62. Final Report Summary - CUPID (Innovative Non-Destructive Corrosion Under Paint Integrated Detection System). *LTD, Insp. Technol. United Kingdom*
63. Magana, D., Parul, D., Brian Dyer, R., And Shreve, A. P. Implementation of Time-Resolved Step-Scan Fourier Transform Infrared (FT-IR) Spectroscopy Using a kHz Repetition Rate Pump Laser. *Appl Spectrosc.* **65**, 535 (2011).
64. VERTEX Series FT-IR Spectrometer. *Bruker Optics* (2017). Available at: https://www.bruker.com/fileadmin/user_upload/8-PDF-Docs/OpticalSpectroscopy/FT-IR/VERTEX/Flyers/VERTEXSerie_Flyer_EN.pdf.
65. Anderson, M. S. *et al.* Fourier transform infrared spectroscopy for Mars science. *Rev. Sci. Instrum.* **76**, (2005).
66. Drag, K. & Lovre, M. Corrosion Investigation of Printing Machines By FT-IR Spectroscopy. *Anal. korozije Tisk. strojeva FT-IR Spektrosk. Metod.* **19**, 899–906 (2012).
67. Namduri H., N. S. Quantitative analysis of iron oxides using Fourier transform infrared spectrophotometry. *Corros. Sci.* **50**, 2493 (2008).
68. Prati, S., Joseph, E., Scitutto, G. & Mazzeo, R. New advances in the application of FTIR microscopy and spectroscopy for the characterization of artistic materials. *Acc. Chem. Res.* **43**, 792–801 (2010).

69. Kendix, E and Prati, Silvia and Mazzeo, Rocco and Joseph, Edith and Sciutto, Giorgia and Fagnano, C. Far infrared spectroscopy in the field of cultural heritage. *Preserv. Sci.* **7**, 8--13 (2010).
70. Vegetation monitoring in Groningen. *T&A Survey Group B.V.* Available at: <http://www.ta-survey.nl/page.php?id=314&lang=EN>.
71. Bruker. Application Note AN #91 HI 90 - Hyperspectral Imaging System. *Bruker Opt.* (2011).
72. Natalia Leone, Mariano Mercurio, Eleonora Grilli, Antonio P. Leone, Alessio Langella, A. B. Potential of vis-NIR reflectance spectroscopy for the mineralogical characterization of synthetic gleys: a preliminary investigation. *Period. di Mineral.* **80**, 433–453 (2011).
73. Torrent, J. & Barrón, V. in *Encyclopedia of surface and Colloid Science 1* 1438–1446 (2002).
74. Scheinost, A. C., Chavernas, A., Barrón, V., & Torrent, J. Use and limitations of second-derivative diffuse reflectance spectroscopy in the visible to near-infrared range to identify and quantify Fe oxides in soils. *Clays Clay Miner.* **46**, 528–536 (1998).
75. Waite, D. M. S. and T. D. Electronic spectra of Fe³⁺ oxides and oxide hydroxides in the near IR to near UV. *Am. Mineral.* (1985).
76. Fernandez, R. N. & Schulze, D. G. Munsell Colors of Soils Simulated by Mixtures of Goethite and Hematite with Kaolinite. *Zeitschrift für Pflanzenernährung und Bodenk.* **155**, 473–478 (1992).
77. Barron, V. & Torrent, J. Use of the Kubelka-Munk theory to study the influence of iron oxides on soil colour. *J. Soil Sci.* **37**, 499–510 (1986).
78. Jepson, W. B. Structural iron in kaolinites and in associated ancillary minerals. *Iron soils clay Miner.* 467–583 (1988).
79. Momma, E. *et al.* Rust classification using image analysis of steel structures. in *2008 3rd International Conference on Sensing Technology* 409–413 (IEEE, 2008). doi:10.1109/ICSENST.2008.4757137
80. Petricca, L., Moss, T., Figueroa, G. & Broen, S. Corrosion Detection Using A.I : A Comparison of Standard Computer Vision Techniques and Deep Learning Model. in *Computer Science & Information Technology (CS & IT)* 91–99 (Academy & Industry Research Collaboration Center (AIRCC), 2016). doi:10.5121/csit.2016.60608
81. Huynh, C. P., Mustapha, S., Runcie, P. & Porikli, F. Multi-class support vector machines for paint condition assessment on the Sydney Harbour Bridge using hyperspectral imaging. *Struct. Monit. Maint.* **2**, 181–197 (2015).
82. *Practical Raman Spectroscopy.* (Springer Berlin Heidelberg, 1989). doi:10.1007/978-3-642-74040-4
83. Bertolucci, H. and. *Symmetry and spectroscopy: an introduction to vibrational and electronic spectroscopy.* (Courier Corporation, 1989).
84. Shebanova, O. N. & Lazor, P. Raman study of magnetite (Fe₃O₄): laser-induced thermal effects and oxidation. *J. Raman Spectrosc.* **34**, 845–852 (2003).
85. Morcillo, M. *et al.* SEM/Micro-Raman Characterization of the Morphologies of Marine Atmospheric Corrosion Products Formed on Mild Steel. *J. Electrochem. Soc.* **163**, C426–C439 (2016).
86. Hanesch, M. Raman spectroscopy of iron oxides and (oxy)hydroxides at low laser power and possible applications in environmental magnetic studies. *Geophys. J. Int.* **177**, 941–948 (2009).
87. Nieuwoudt, M. K., Comins, J. D. & Cukrowski, I. The growth of the passive film on iron in 0.05 M NaOH studied in situ by Raman micro-spectroscopy and electrochemical polarisation. Part I: near-resonance enhancement of the Raman spectra of iron oxide and oxyhydroxide compounds. *J. Raman Spectrosc.* **42**, 1335–1339 (2011).
88. Strommen, D. P. & Nakamoto, K. Resonance raman spectroscopy. *J. Chem. Educ.* **54**, 474 (1977).
89. Martin, T. P., Merlin, R., Huffman, D. R. & Cardona, M. Resonant two magnon Raman scattering in α -Fe₂O₃. *Solid State Commun.* **22**, 565–567 (1977).
90. Winkler, J. *Titanium dioxide.* (Vincentz Network, 2003).

91. Hardcastle, F. D., Ishihara, H., Sharma, R. & Biris, A. S. Photoelectroactivity and Raman spectroscopy of anodized titania (TiO₂) photoactive water-splitting catalysts as a function of oxygen-annealing temperature. *J. Mater. Chem.* **21**, 6337 (2011).
92. Senesi, G. S. Laser-Induced Breakdown Spectroscopy (LIBS) applied to terrestrial and extraterrestrial analogue geomaterials with emphasis to minerals and rocks. *Earth-Science Rev.* **139**, 231–267 (2014).
93. Rohwetter, P. *et al.* Filament-induced remote surface ablation for long range laser-induced breakdown spectroscopy operation. *Spectrochim. Acta Part B At. Spectrosc.* **60**, 1025–1033 (2005).
94. Wiens, R. C. *et al.* The ChemCam Instrument Suite on the Mars Science Laboratory (MSL) Rover: Body Unit and Combined System Tests. *Space Sci. Rev.* **170**, 167–227 (2012).
95. Elhassan, A. Short Review Of Laser-Induced Breakdown Spectroscopy For Corrosion Diagnostic. in *AIP Conference Proceedings* **1380**, 65–69 (2011).
96. Olympus scientific solutions Americas. Terra X-ray diffraction and x-ray fluorescence analyzer (User's manual). (2014).
97. Chiari, G., Sarrazin, P. & Gailhanou, M. A portable non-invasive XRD-XRF instrument for the study of art objects. in *Denver X-Ray Conference. JCPDS-International Centre for Diffraction Data USA* **23**, 175–186 (2008).
98. Sarrazin, P. *et al.* Field deployment of a portable X-ray diffraction/X-ray fluorescence instrument on Mars analog terrain. *Powder Diffr.* **20**, 128–133 (2005).
99. NASA Technology. Mineral Analyzer Shakes Answers Out of Soil and Rocks. Available at: https://spinoff.nasa.gov/Spinoff2017/ee_6.html.
100. Scaling and Corrosion Residue Identification with X-ray Diffraction. *Olympus Corporation* (2017). Available at: <https://www.olympus-ims.com/en/applications/scaling-and-corrosion-residue-identification-with-x-ray-diffraction/>.
101. Nummi, E. Analysis of silicon in steel using the Thermo Scientific Niton XL5 analyzer to prevent sulfidic corrosion failures. *Thermo Sci. Appl. Note* (2016).
102. Calvero. Schematic representation of X-ray fluorescence. (2006). Available at: https://en.wikipedia.org/wiki/File:X-ray_fluorescence_simple_figure.svg.
103. Wikipedia, L. at E. File:XRFScan.jpg. (2009). Available at: <https://en.wikipedia.org/wiki/File:XRFScan.jpg>.

5. Acknowledgements

DFM A/S acknowledges funding from the Danish Agency for Institutions and Educational Grants as part of the result contract “Dronemetrologi”, from the EU regional fund for regional development and the region of southern Denmark (Syddansk Vækstforum).